Development of a photon-counting near-fano-limited x-ray CMOS image sensor for THESEUS' SXI

Conference or Workshop Item

Development of a photon-counting near-Fano-limited X-ray CMOS Image Sensor for THESEUS' SXI

Julian Heymes[a], Konstantin Stefanov[a], Matthew Soman[a], Davide Gorret[b], David Hall[a], Kyriaki Minoglou[c], David Morris[b], Jérôme Pratlong[b], Thibaut Prod'homme[c], Georgios Tsiolis[b], and Andrew Holland[a]

[a]Centre for Electronic Imaging, The Open University, Milton Keynes MK7 6AA, United Kingdom
[b]Teledyne-e2v, 106 Waterhouse Lane, Chelmsford CM1 2QU, United Kingdom
[c]ESA-ESTEC, P.O. Box 299, 2200 AG Noordwijk, The Netherlands

ABSTRACT

THESEUS (Transient High Energy Sky & Early Universe Surveyor) is one of the three candidates for the M5 mission of the European Space Agency. The favoured mission will be announced in 2021 for an expected launch in 2032. THESEUS will be equipped with a Soft X-ray Imager (SXI) composed of a set of two telescopes using micro-pore optics offering an overall field of view of 0.5 sr (<2' accuracy) for X-ray energies between 300 eV and 5 keV. The focal plane of each SXI telescope has a 16 x 16 cm^2 cooled detector area. However, the limited radiator accommodation on the spacecraft prohibits the use of CCDs since cooling the focal planes to an optimal temperature for radiation hardness (<-100 °C) is not feasible. Therefore, the development of a suitable CMOS Image Sensor (CIS), capable of handling the expected levels of radiation at higher operating temperatures (approximately -30 °C) has been proposed. To demonstrate the performance required for the THESEUS SXI detector, a 2 x 2 cm^2 prototype is under development using Open University pixel designs in a Teledyne-e2v digital CMOS platform. The pixel design will allow full depletion over silicon thickness of 35 µm for optimal soft X-ray quantum efficiency and instrument background suppression, and will be capable of near-Fano-limited spectral resolution that will also be of prime interest for synchrotron and Free Electron Lasers (FEL) applications. In this paper, we will present the design considerations and simulations leading to the implemented structures complying with THESEUS' SXI requirements.

Keywords: CIS, CCD, Soft X-ray, SXI, THESEUS, Spectrometer, Photon counting

1. INTRODUCTION

Silicon image sensors have become the detector of choice for many projects operating in the visible, UV/EUV and X-ray bands due to the combination of high detection efficiency, low noise, uniformity, area etc. In the field of X-ray applications, the Charge-Coupled Device (CCD) has been the workhorse detector for astronomy missions such as for the X-ray Multi Mirror Mission[1] (XMM), Swift,[2] Chandra,[3] and more recently the Soft X-ray Imager (SXI) on the SMILE mission.[4] In all of these missions, the CCD arrays are susceptible to radiation damage from energetic protons, which degrades the Charge Transfer Efficiency (CTE) of the device. This in-turn can lead to a degradation of the X-ray energy resolution and effective sensitivity of the sensors. To mitigate the effects of the damage, the CCDs are cooled to an operating temperature of between -60 °C to -130 °C, locking charge in the proton-induced traps so that the charge generated by the X-rays can be read out with a more tolerable degradation which is within the specification of the mission requirements.

However, the resources available to the THESEUS spacecraft will only be capable of cooling the focal plane of the SXI to a minimum temperature of around -30 °C. Studies for the SMILE SXI instrument have demonstrated that for the anticipated level of Total Non Ionising Dose (TNID)-induced damage, a CCD-based instrument

Further author information: (Send correspondence to J.H.)
J.H.: E-mail: julian.heymes@open.ac.uk, Telephone: +44 (0)1908 655351

would lose the ability to sense soft X-ray photons progressively into the mission.[4] This ultimately led to the baselining of a less mature solution based on scientific CMOS Image Sensors (CIS).

The developments needed toward realising an imaging sensor of large area, high detection efficiency, low noise and good X-ray spectroscopy are very complementary between the earlier CCD technology and the newer scientific CMOS imager technology. Structures developed for previous devices and specific developments can be integrated into a single detector as a prototype for the THESEUS SXI instrument. CIS have advanced considerably throughout the past two decades, offering noise performance comparable to CCDs, low dark current (using the pinned photodiode) and a linear response over a large dynamic range. Despite these advances, further developments are required to meet the science requirements of the THESEUS SXI. In particular, larger pixels are required (40 µm) with a fully depleted thicker device substrate (>35 µm) to efficiently collect the signal from the X-ray photons, and an Optical light Blocking Filter (OBF) to avoid stray light contamination. When combined with low noise, the sensor can approach the so-called "Fano-limited" performance, providing high-resolution spectroscopy on the X-ray photons.

The use of the CMOS image sensor technology introduces a couple of additional benefits. The in-pixel signal manipulation with CIS technology has only one transfer operation: from the photodiode collecting the signal to the sensing node. This avoids the CCD technology's "Achilles Heel" of radiation-induced degradation to the charge transfer efficiency. This enables large arrays to be constructed, with no link between array size and damage. The CIS technology has similarities to a CCD sense node and can operate with very low current, yielding large area sensors which can operate both with high frame rates, and with very low power. This ability of the CIS technology to enable large imaging arrays with low operating power, has a very significant advantage for the instrument cooling requirements, enabling focal plane operating temperature of -30 °C to be achieved, for all SXI telescopes, with the modest cooling resources available to the spacecraft.

In this paper we present the development of a high-performance soft X-ray photon counting spectrometer based on CMOS image sensor technology, led by the Open University in collaboration with Teledyne-e2v. The device will feature the deep depletion extensions (DDE) and backside bias demonstrated with the BSB1 prototype[5] capable to deplete several tens of micrometres. The prototype array will be 2 x 2 cm^2, will operate with near Fano-limited spectral resolution, high detection efficiency, and at high frame-rate. The technology will be scalable to realise an image sensor of 4 x 8 cm^2, which when built into a 2 x 4 mosaic array will produce the largest imaging X-ray spectroscopy array ever flown. The technology will also find use in terrestrial applications such as synchrotron research and free electron lasers (FELs). In addition, some of the technologies developed can be used in other astronomy applications (e.g. low noise, larger pixels which are fully depleted with improved red-response, etc.).

2. THE THESEUS SOFT X-RAY IMAGER

The Transient High Energy Sky and Early Universe Surveyor (THESEUS),[6] is one of the mission concepts selected to enter assessment phase study for the European Space Agency's 5^{th} medium-class (M5) mission within its Cosmic Vision Programme. The downselected mission will be announced in 2021.

If selected, THESEUS is expected to be launched in 2032 in a low inclination low earth orbit (LEO, ≈600 km, <5 °) to explore the Early Universe, up to z≈ 10, by unveiling a complete census of the Gamma-Ray Burst population in the first billion year, and to perform an unprecedented deep monitoring of the X-ray transient Universe.

The expected instrumentation payload of THESEUS is composed of:

- the *InfraRed Telescope* (IRT, λ=0.7 µm–1.8 µm),
- the *X-Gamma rays Imaging Spectrometer* (XGIS, E=2 keV–20 MeV), and
- the *Soft X-ray Imager* (SXI, E=300 eV–5 keV).

The SXI instrument (led by the University of Leicester, UK) is planned to be composed of two telescopes using micro-pore optics to focus incoming X-rays onto an imaging X-ray sensor array over a field of view of 0.5 sr with a source location accuracy of better than 2 arcmin. Each of the focal plane arrays of each telescope will be the largest X-ray photon-counting arrays ever flown (16 x 16 cm^2).

3. CIS221-X: A PROTOTYPE CIS FOR THESEUS SXI

The flight model soft X-ray imager on THESEUS requires a detector focal plane with a high sensitivity in the energy range 300 eV to 5 keV. A focal plane of monolithic CMOS Image Sensors from Teledyne-e2v is proposed, combining building blocks demonstrated in their CMOS digital platform development[7] with pixel designs optimised for the soft X-ray energy range. The devices will be back-thinned at Teledyne-e2v and Optical light blocking filters will be deposited to prevent stray light while ensuring high soft X-ray transmission.

The Teledyne-e2v CAPELLA sensor is a science-grade imager featuring 2048 × 2048 10 µm pixels. The CAPELLA device is multi-purpose and has a Charge-to-Voltage Factor (CVF) of 40 µV/ e^- and ≈ 6 e^- RMS noise. The device includes design elements from Teledyne-e2v's latest digital platform development and includes column ADCs with up to 14-bit resolution, which can be degraded to 10-bit with corresponding increases in readout speed. The architecture has been designed for high immunity to single event effects in the space environment. In its native 2k x 2k format the device can operate at up to 20 fps. A HiRho version of the CAPELLA sensor, capable of fully depleted operation and named the CIS220, has been developed by Teledyne-e2v based on the DDE technology successfully demonstrated with the BSB1 prototype sensor.[5]

The 2 x 2 cm^2 prototype sensor, designated as CIS221-X, is based on the CAPELLA/CIS220 architecture with changes to the pixel design to satisfy the required specification for the THESEUS SXI. The three main differences in the architecture are:

- An increase of the pixel pitch from 10 µm to 40 µm for improved energy resolution through less charge splitting, conveniently occupying the space of 4 x 4 standard CAPELLA/CIS220 10 µm pixels to minimise the re-design effort towards demonstrating the soft X-ray detection capabilities.
- A thicker, fully depleted sensitive volume, nominally 35 µm, for background rejection, and for high quantum efficiency up to 5 keV.
- A redesigned transfer gate and sense node combination for higher CVF (increased from 40 µV/ e^- to >90 µV/ e^-), as well as the use of low noise processes to achieve <5 e^- RMS.

Another change to the device includes the incorporation of an optical light blocking filter for stray light rejection while guaranteeing high soft X-ray quantum efficiency and high vacuum stability.

The reduction in total row count from the pitch increase, together with digitisation to only 12 bits, should enable a frame rate of 100 fps that would require a re-design to match the row addressing and readout ADCs to the physical pixels. A future 4 x 8 cm^2 sensor with 40 µm pixels should be capable of readout at 50 fps without degradation in performance, which will provide greater tolerance to stray light and dark current; the latter enabling relaxation of the operating temperature specification for the focal plane arrays. However, due to camera electronics limitations, the baseline frame rate for the SXI is 10 fps.

The incorporation of all three design modifications onto a single pixel design represents a unique challenge since there is typically trade-off between performance in each area. CMOS image sensors are known to suffer from a phenomenon referred as "image lag" whereby there is incomplete charge transfer from the Pinned Photodiode (PPD) to the sense node. Increasing the size of the pixel without modification to the transfer gate and/or the PPD structure can result in increased image lag, as can reducing the size of the sense node to improve the noise performance. A large pixel with low noise will therefore require a novel design to maintain the charge transfer performance.

To implement each of the changes, a single sensor was designed with four different pixel variants within the CAPELLA/CIS220 architecture (Figure 1). Three of these variants have 40 µm square pixels and have modifications to the PPD and the transfer gate structure to improve image lag and noise performance. The fourth variant has a 10 µm pixel pitch and will serve as a reference. All four variants feature the deep depletion implants as well as new transfer gate and sense node combination for high CVF. The OBF will be incorporated on 50 % of the sensor, covering all four variants but only deposited from the centre to one edge of the device. The remaining 50 % of the sensor will be uncoated silicon, acting as a control to enable detailed characterisation of the X-ray and optical transmission.

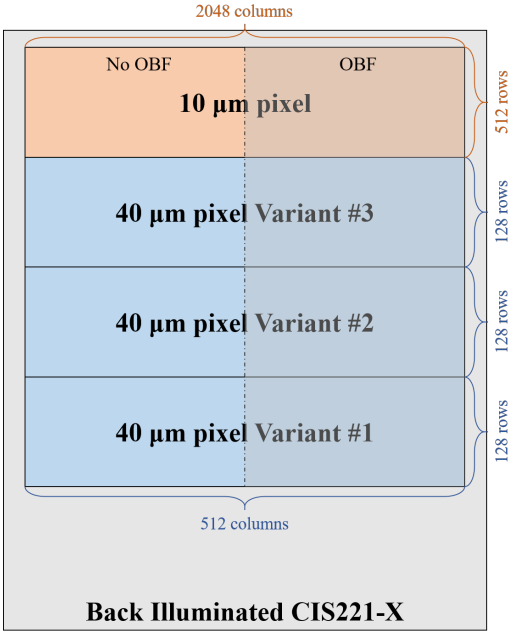

Figure 1. Schematic representation of CIS221-X architecture with three 40 µm pixel variants and one 10 µm. The boundary of the Optical light Blocking Filter (OBF) is shown as the dash-dotted line.

4. CIS221-X PERFORMANCE MODELLING

4.1 LOW CAPACITANCE SENSE NODE FOR LOW NOISE

Effectively detecting soft X-rays in the 0.3 keV–1 keV range, particularly where some of the signals from the absorbed photons may be split over several pixels, requires very low noise. For XMM, an operational noise of $\approx$ 3.5 e^- RMS was obtained. However, for the image readout of a CCD, all pixels are sampled by the same analogue chain, making the resulting image to have a single noise value. In the case of CMOS image sensors, each pixel has its own noise behaviour, and this produces a distribution of noise values, so a single parameter to capture noise behaviour is not suitable.

To achieve a low noise using a CIS one must consider the noise behaviour of the Field Effect Transistors (FETs) making up the amplification chain and the Analog-to-Digital Converter (ADC). The amplification of the signal chain can be broken down into the gain of the amplifiers within the pixel, together with any additional gain in the column amplifiers. This combination results in a pixel "responsivity" or charge-to-voltage conversion factor (CVF). One of the key challenges toward making a low-noise CIS, requiring a high value for the CVF, is to reduce the sense node capacitance, whilst retaining good charge transfer to the sense node, and low lag.

If one adopts a similar approach to that for XMM, then one would like the bulk of the pixels in the image to have a noise value around 3.5 e^- RMS, and preferably lower, which helps with event detection and charge characterisation. Due to outlier pixels, which have the higher noise values, it is also necessary to specify the maximum number of pixels which should exceed a certain value. The requirement for this development is that >90 % of pixels should have a noise <5 e^- RMS.

In Figure 2 we show noise histograms and cumulative pixel plots for a CAPELLA sensor manufactured using the same process as for CIS221-X. CAPELLA is a general-purpose sensor, designed and optimised for combined noise, full well, and dynamic range considerations. In the case of an X-ray photon counting spectrometer, where the largest signal might be $\approx$ 3000 e^- from a single photon, the FWC does not need to be high and one can increase the pixel CVF to achieve low noise. For the new CIS221-X design the pixel sense node capacitance was reduced from that of CAPELLA to achieve >90 µV/e^-. Figure 2 also includes the noise distributions and cumulative plots for the predicted noise of the CIS221-X, plus a version which includes a 20 % margin on the

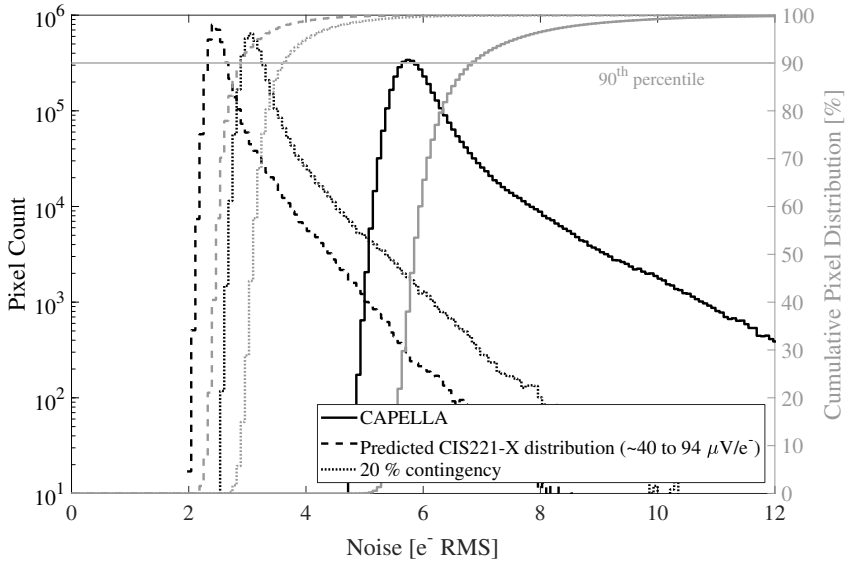

Figure 2. Noise estimates for the CIS221-X pixels based on new data from a CAPELLA device

estimated CVF value of 94 µV/ e⁻ (see Section 5). This data shows that the noise requirement of more than 90 % of pixels having a noise value of no more than 5 e⁻ RMS should be met, and is also below the 3.5 e⁻ RMS achieved for the XMM/EPIC instrument.

4.2 DARK CURRENT AND DEVICE OPERATING TEMPERATURE

The pinned photodiode pixel inherently has a low dark current at beginning of life (BOL), and the dark current induced by radiation effects becomes the main driver on the operational temperature requirements. For THESEUS SXI, the dark current requirement is to ensure that the shot noise from dark signal is not a significant contribution to the overall noise budget, and to avoid the generation of false triggers and the pollution of the data stream. From a nominal readout noise performance of 3.5 e⁻ RMS, an average dark signal of 12.25 e⁻pixel^{-1} would result in an equal contribution from readout noise and dark signal, and is therefore chosen as a comparative threshold in the following analysis. At a range of example frame rates, the dark current limits required to meet the 12.25 e⁻pixel^{-1} threshold is shown in Table 1.

Table 1. Dark current requirements for a range of THESEUS detector frame rates, calculated from a nominal dark signal threshold of 12.25 e⁻pixel^{-1}

Bit Depth	**Frame Rate**	**Dark Current Limits to meet 12.25 e⁻pixel^{-1}**	**Comment**
-	0.5 fps	6.1 e⁻s^{-1}	
10	6.2 fps	75.9 e⁻s^{-1}	CAPELLA (8 cm x 4 cm, 10 µm)
10	10 fps	122 e⁻s^{-1}	Development CIS (8 cm x 4 cm, 40 µm)
10	20.1 fps	247 e⁻s^{-1}	Development CIS (8 cm x 4 cm, 40 µm)
12	39.3 fps	481 e⁻s^{-1}	Development CIS (8 cm x 4 cm, 40 µm)

In radiation studies of Teledyne-e2v CIS for other missions, such as the CIS115 for JANUS,[8] the BOL dark current and Total Ionising Dose (TID)-induced dark current has been insignificant compared to the increase in bright pixel defects induced by the TNID radiation environment.[9,10] The increased pitch and depleted volume in the CIS221-X (when compared to the partially depleted 7 µm pixel of the CIS115) will increase the dark current defect density per pixel, and therefore it is even more critical to understand the effect of TNID-induced dark current defects on the overall imager performance. The detailed analysis of the TNID-induced CIS115 bright pixel defect has been utilised to build a model for the THESEUS pixel and radiation environment. The model

has been scaled using an estimated end of life (EOL) equivalent fluence of 2 x 10^9 protons(10 MeV) cm^{-2}, and evaluated at the dark signal threshold and frame rates presented in Table 1. The percentage of the focal plane pixels that are expected to contain a TNID-induced bright pixel defect is shown as a function of operational temperature in Figure 3. A focal plane with 40 µm pixels operating at 10 fps can be expected to lose >1 % of its pixels to bright pixel defects at EOL when operating above -33.5 °C. The model is based on many assumptions, and will be assessed experimentally, but gives an indication of appropriate performance in the -40 °C to -30 °C range.

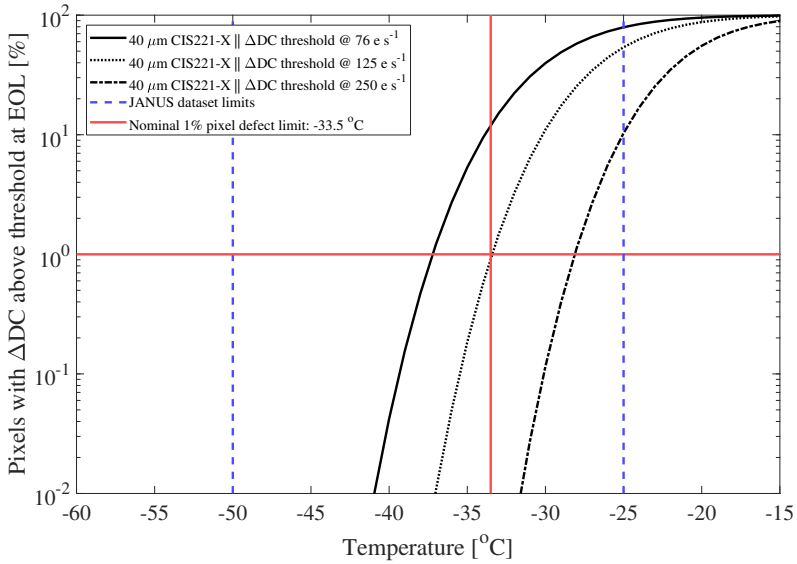

Figure 3. Probabilities of pixels with ΔDC (change in dark current) being above the X-ray detection threshold for a range of different configurations based on experience from the JANUS CIS115; indicating that an operation temperature of below -33.5 °C should be sufficient

4.3 SOFT X-RAY QUANTUM EFFICIENCY

In order to avoid stray light contamination on the focal plane, the back-illuminated passivated devices must be coated with an OBF. The coating consists of a deposited thin film composed of mostly aluminium which affects the Quantum Efficiency (QE). Therefore, the soft X-ray QE with and without OBF for CIS221-X has been modelled to observe the effect of the added material at the back-surface of the passivated device and is shown in Figure 4. The parameters used and the margins for the modelling of the passivation and the OBF are given in Table 2.

Table 2. Parameters used to model the predicted soft X-ray Quantum Efficiency of the CIS221-X

Parameter	**Passivation only**			**Passivation + OBF**		
	Min QE	**Nom QE**	**Max QE**	**Min QE**	**Nom QE**	**Max QE**
SiO2 thickness	2.5 nm	2 nm	1.5 nm	2.5 nm	2 nm	1.5 nm
P+ layer (Passivation)						
Sensitive Si	34 µm	35 µm	36 µm	34 µm	35 µm	36 µm
OBF Composition	-	-	-	Less Al	Al alloy	100 % Al
OBF Thickness	-	-	-	Nom + 10 nm		Nom - 10 nm

The OBF will be made of an aluminium alloy. A very small variation in the element ratio can be expected (<1 %) and the thickness is not expected to vary over more than 10 nm of the nominal thickness. However, a much smaller proportion of aluminium in the alloy has been considered as the worst case for the model. Very

high QE (above 80 %) can be expected between 100 eV and 5 keV for uncoated devices and between 500 eV to 5 keV for coated devices.

Soft X-ray QE data have been previously measured for the enhanced passivation using back illuminated CCD97s,[11] giving an indication of the back surface process performance without OBF. The data points from two CCD97 devices (15051-7-3 and 15051-7-7) are also shown on Figure 4 for energies up to 1 keV, where the performance is dominated by the back surface process (and overall detector thickness is not significant). Their efficiency with the addition of an OBF has also been calculated. As these devices are known to have been adversely affected by a manufacturing process issue[12] (now recognized and corrected), the performance of a typical production device is expected to be slightly better than that shown in the data of Figure 4, particularly at the lower energies where the attenuation length is shortest.

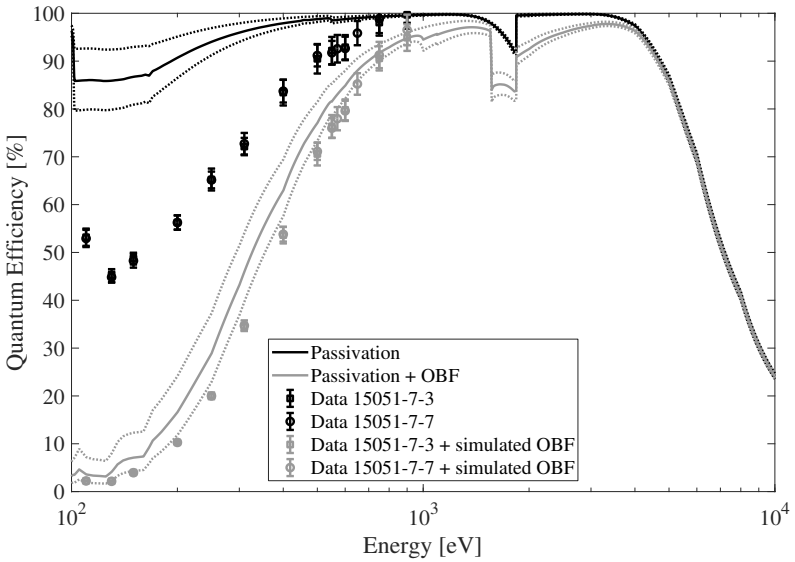

Figure 4. Estimation of the Soft X-Ray Quantum Efficiency of CIS221-X with and without a nominal OBF. Experimental data points of non-coated passivated CCD97s are shown as a reference. The data points with OBF are estimated by adding the nominal contribution of the coating to the QE.

4.4 ENERGY RESOLUTION

The energy resolution in the soft X-ray spectral range is predicted in figure 5 using the key contributors, and assuming singe pixel charge collection without additional loss mechanisms such as trapping at the back-surface or image lag. The components considered are the sensor readout noise, the silicon Fano-limited shot noise as well as the inter-pixel calibration differences that can supposedly be reduced by thorough calibration.

Within the spectral range of interest of the SXI, the main contributor to the energy resolution is the Fano noise followed by the readout noise below 1 keV. Above this energy limit, the second main contributor to the energy resolution of CIS221-X is the pixel-to-pixel response non-uniformity. Overall, the energy resolution is near-Fano-limited, providing high-resolution spectroscopy on the X-ray photons.

5. DESIGN OF SOFT X-RAY OPTIMISED PIXELS

The deep depletion capabilities of CIS221-X are made possible using a n-doped buried layer, the deep depletion extension (DDE), and further described in.[5] By varying the implantation energy of the DDE, the depth of the buried layer can be tuned which can affect the leakage current under reverse bias. The BSB1 and CIS220 devices were fabricated with three different variants of DDE implants: "shallow", "medium", and "deep". The same implants parameters have been baselined for the development of CIS221-X.

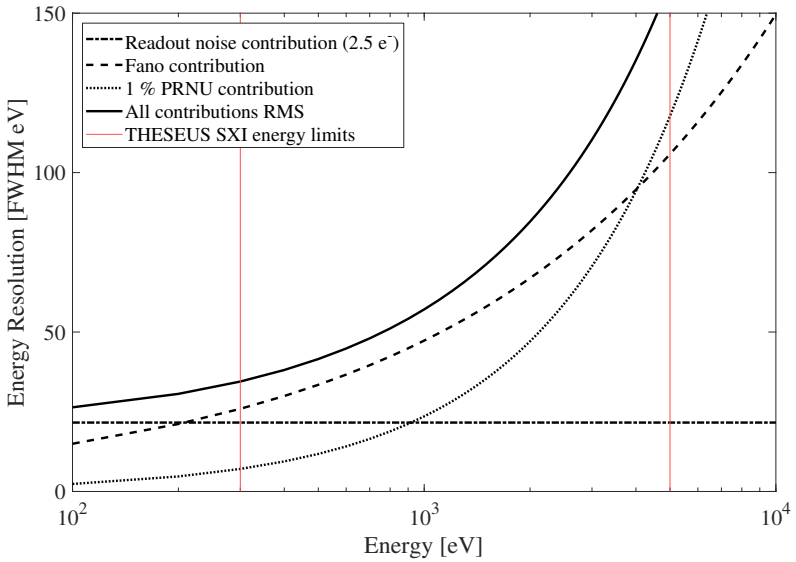

Figure 5. X-ray energy resolution expressed as FWHM vs. energy showing the contributions from the different physical processes.

The pixel variants occupy 4 sub-arrays along with equal areas, as shown in Figure 1. All variants have an increased CVF over the CIS220 pixel to achieve the lower noise required. The improved responsivity is made possible by using a smaller transfer gate and a very small sense node. The CVF was calculated from the capacitances of the sense node and the source follower using the process parameters and the extracted parasitic capacitance from the layout. The total calculated sense node capacitance is 1.55 fF, of which 0.6 fF is parasitic, giving output CVF of 94 µV/ e⁻. The estimated readout noise from the source follower is 1.9 e⁻ RMS.

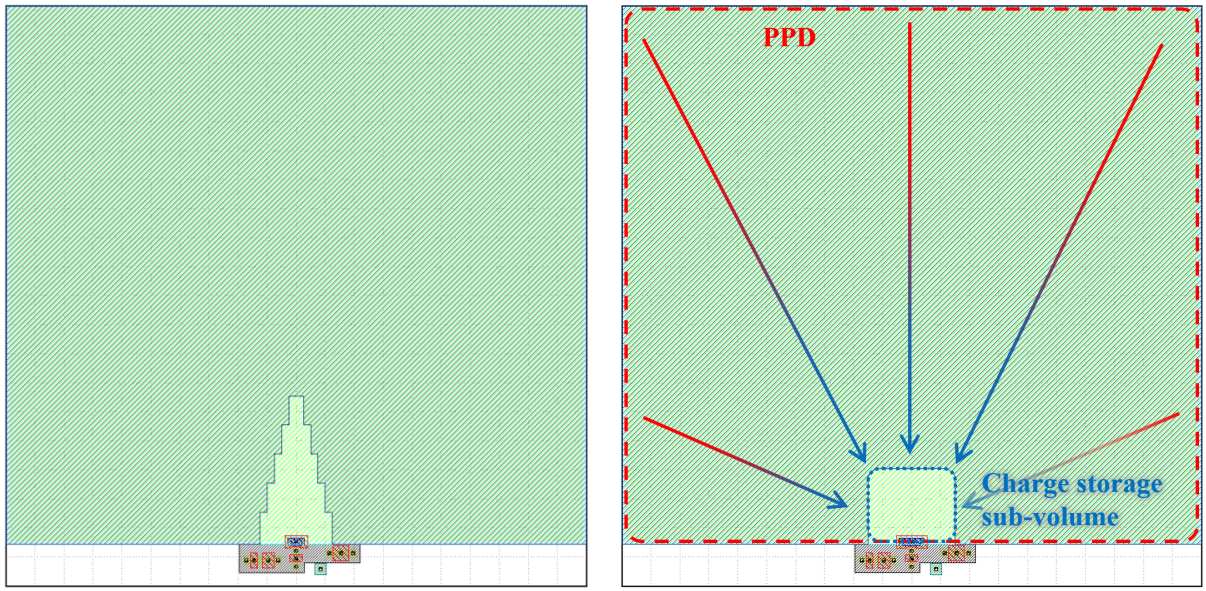

Figure 6. Layouts of two of CIS221-X's pixel variants. (left): 40 µm Variant #2. (right) 40 µm Variant #3 with annotations showing the charge concentration within the sub-volume next to the transfer gate. The additional pinning implant is drawn with a hatched blue mask.

The goal of the 40 µm pixel variants is to collect the majority of the X-ray-generated signal, resulting in most X-rays having their signal sampled by a single pixel – which helps achieve high spectral resolution and sensitivity to low X-ray energies. In the enlarged pixels, the collected charge is stored over the large area of the photodiode. Therefore, since charge transfer relies on diffusion this can ultimately cause severe image lag. With additional pinning implant, the charge packet can be concentrated towards the transfer gate and be held within a small area. A layout for two pixel variants are shown in Figure 6 where a single additional pinning implant layer is drawn with a hatched blue mask. The annotations over the layout on the right side of Figure 6 shows the principle of charge concentration in a reduced area next to the transfer gate. A schematic cross-section of an enlarged pixel with DDE implants and a single additional pinning implant is shown in Figure 7.

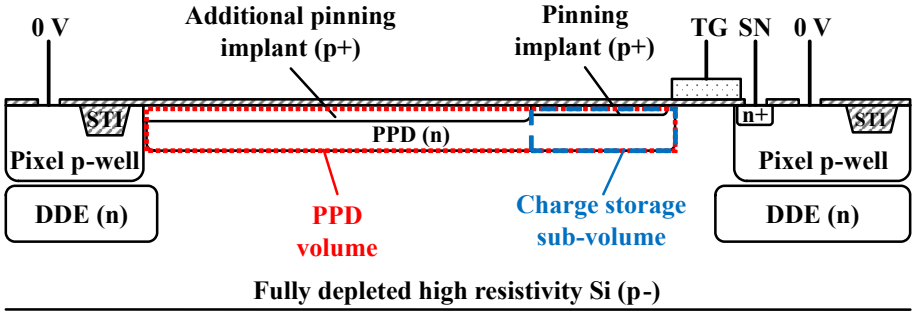

Figure 7. Schematic cross section of a CIS pixel with DDE implants and additional pinning implant.

The pixel variants of CIS221-X are:

- 10 µm pitch pixel with DDE for depletion for a measurement of the charge splitting and image lag.
- "Variant #1" - A 40 µm pitch pixel with an additional pinning implant to channel the collected charge towards the transfer gate for storage within a small area and hence allow rapid charge transfer to the sense node.
- "Variant #2" - A 40 µm pitch variant with a variation of the shape of the additional pinning implant ("Christmas Tree") to help aid rapid charge transfer to the sense node (layout shown in figure 6 left).
- "Variant #3" - A 40 µm pitch variant like Variant #1 with a larger transfer gate for potentially better lag performance with a similar CVF. (layout shown in figure 6 right). This variant also differs from the others by using an additional process to reduce the noise.

5.1 REVERSE BIAS

The soft X-ray detection performance of CIS221-X highly relies on the fully depleted operation of the device made possible by the combination of the DDE layer, a high resistivity substrate (>1000 Ω cm), and adequate reverse biasing. Calculations of the depletion depth of a pn-junction[13] indicate that the device would be fully-depleted with a minimum reverse bias of -11 V. It is however preferred to operate the device in an over-depleted mode to guarantee a non-zero electric field at the very back of the device. An adequate bias for the device to be in such state is approximately -20 V.

TCAD simulations using the Synopsys Sentaurus TCAD tools[14] and the pixel layout files were conducted to determine the breakdown voltage of each DDE variant. As a verification measure, simulations of the CIS220 pixel configuration were performed and compared to initial measurements results. The similarities in the observed trends confirmed the model and gave confidence the model's suitability to determine the behaviour of different the DDE implant energy options in the CIS221-X.

Simulations of the reverse current for the small and large CIS221-X pixels variants are shown in Figure 8.

With the shallow DDE implant, the breakdown voltage is much below the full depletion voltage. The medium variant is the minimum that can be considered despite the shoulder being below the required bias. However,

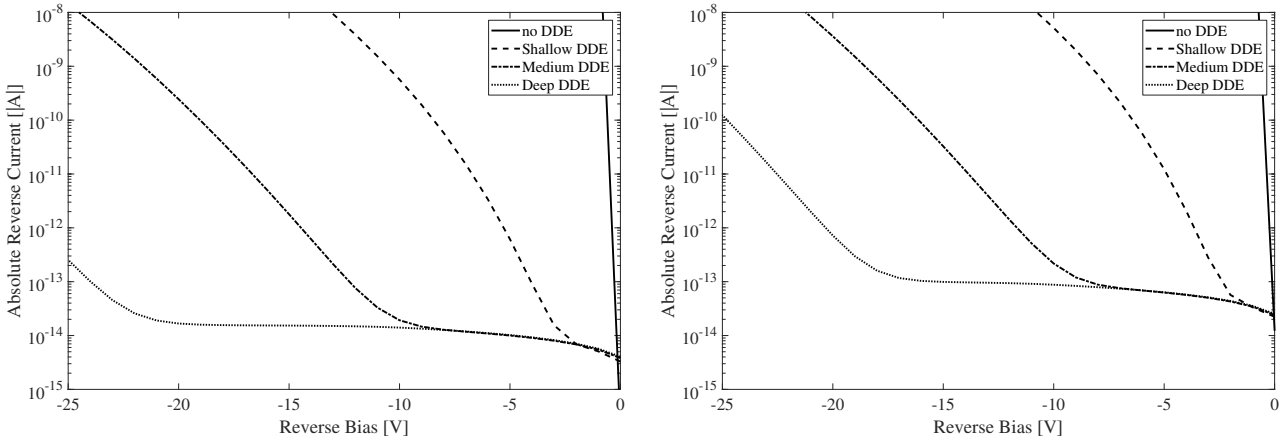

Figure 8. Simulated reverse current in a 10 µm pixel (left) and in a 40 µm pixel (right) with 3 different DDE variants (shallow, medium, and deep), and without DDE as reference.

the current remains acceptable beyond the breakdown limit as long as the total reverse current in the whole 2 x 2 cm^2 array remains below ≈ 1 mA. The simulations indicate that the best variant for CIS221-X is therefore the deep implanted DDE. Both the medium and deep variants have been chosen for fabrication.

5.2 CHARGE COLLECTION AND TRANSFER

Transient simulations of the 40 µm pixels were also conducted to observe the effects of one or more additional pinning implant on charge collection and transfer. For the observation of the movement of the charge packet in the PPD, two regions were probed in the pinned photodiode. The first corresponds to the whole PPD volume (shown as the areas delimited by red lines in Figure 6 right and 7), represented as red lines for both plots in figure 9, while the second is limited to the charge storage sub-volume (shown as the areas delimited by blue lines in Figure 6 right and 7) next to the transfer gate represented with blue lines in figure 9. Four pinning configurations were tested represented by different line styles: no additional pinning implants, and with up to 3 additional implants added further away from the transfer gate.

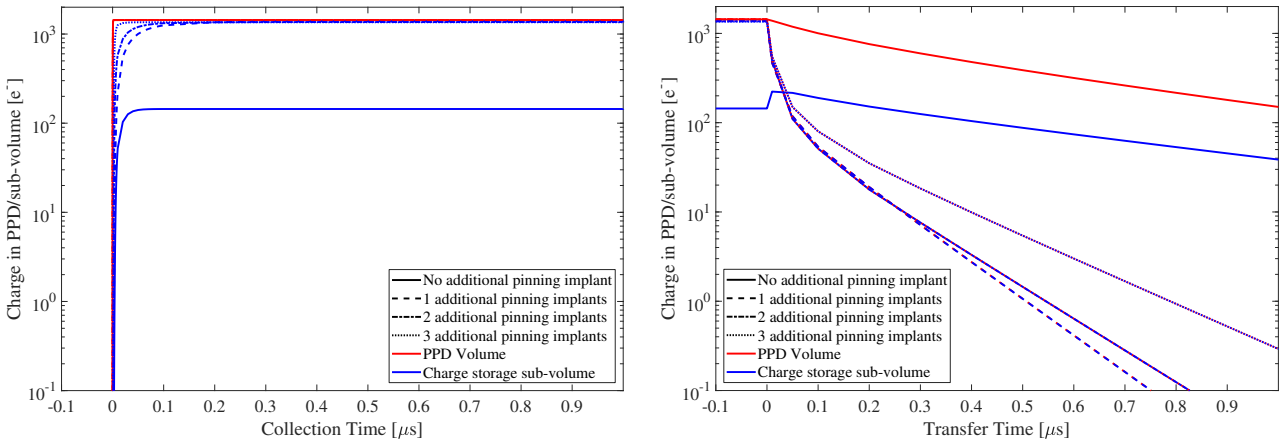

Figure 9. Transient simulations of multiple configurations of additional pinning implants (1, 2, and 3) in a 40 µm pitch pixel variant. (left) Charge collection simulation. (right) Charge transfer simulation.

Charge collection (Figure 9 left): At t=0 s, a charge is generated in the sensitive volume and is entirely collected in the PPD. Additional pinning implants allow charge concentration in the sub-volume right next to

the transfer gate in less than 300 ns. With no additional pinning implant, the charge remains stored in the whole PPD.

Charge transfer (Figure 9 right): At t=0 s, charge transfer begins. The charge is transferred in less than 1 µs in a structure with additional pinning implants and remains incomplete without any additional implant (which would manifest as image lag). It is however important to mention that the simulations, especially the transfer times, are only indicative and not representative of the actual performance as the precise parameters of the foundry's process are proprietary. Nevertheless, the simulation results show that one additional pinning implant is sufficient to guarantee efficient charge transfer in 40 µm pixels.

6. CONCLUSIONS AND FUTURE WORK

The development of a prototype detector is underway to demonstrate the performance of a CMOS Image Sensor optimised for soft X-ray detection, in a digital architecture designed for space applications. The read noise, pixel pitch, sensitive silicon thickness and image lag performance have been specified and designed for future instrumentation such as the Soft X-ray Imager on THESEUS. This solution in CMOS technology has the potential to offer equivalent or better performance than the traditional CCD focal plane solution, whilst requiring significantly less cooling resource from the spacecraft, reducing the system-level mass, power and weight.

The CIS221-X device, based on Teledyne-e2v's CIS220, embeds 4 pixel variants: a 10 µm pitch pixel and three 40 µm pitch variants optimised for X-ray photon spectroscopy. The low noise and high CVF design will allow near-Fano-limited spectroscopic performance in the soft X-ray spectrum. One half of the passivated back-illuminated device will be coated with an optical light blocking filter for stray light rejection

The fully depleted operation of the device is made possible using the Deep Depletion Extension technology demonstrated in BSB1 and applied to Teledyne-e2v's CIS220. Simulations have demonstrated that over-depleting a 35 µm thick silicon substrate with 1000 Ω cm resistivity requires a reverse bias of 20 V.

Minimising image lag in large pixels require additional pinning implants to concentrate the collected charge towards the transfer gate within a small area equivalent to a 10 µm pitch pixel. Transient TCAD simulations have been used to show that at least one additional implant is required to guarantee charge concentration in less than 300 ns to allow full charge transfer within 1 µs.

The 2 x 2 cm^2 prototype sensors are being manufactured in two different variants (medium and deep DDE) and will be available for initial front-illumination testing in the first half of 2021. Back-thinning, passivation, and deposition of optical light blocking filters will be performed by Teledyne-e2v to provide back-illuminated devices to be characterised by the SXI instrument consortium as of the summer of 2021 to reach TRL 5/6 by 2024.

ACKNOWLEDGMENTS

This programme is funded by ESA under the E/0901-01 Technology Development Element "CMOS Image Sensor for X-ray Applications".

The THESEUS SXI instrument is being led by Prof. Paul O'Brien and Dr. Ian Hutchinson, University of Leicester, UK.

REFERENCES

[1] M. J. L. Turner *et al.*, "The European Photon Imaging Camera on XMM-Newton: The MOS cameras," *Astronomy & Astrophysics* **365**, pp. L27–L35, Jan. 2001.

[2] D. N. Burrows *et al.*, "The Swift X-Ray Telescope," *Space Science Reviews* **120**, pp. 165–195, Oct. 2005.

[3] G. P. Garmire *et al.*, "Advanced CCD imaging spectrometer (ACIS) instrument on the Chandra X-ray Observatory," in *X-Ray and Gamma-Ray Telescopes and Instruments for Astronomy*, J. E. Truemper and H. D. Tananbaum, eds., **4851**, pp. 28 – 44, International Society for Optics and Photonics, SPIE, 2003.

[4] M. Soman *et al.*, "The SMILE soft x-ray imager (SXI) CCD design and development," *Journal of Instrumentation* **13**, pp. C01022–C01022, Jan 2018.

[5] K. Stefanov *et al.*, "Design and Performance of a Pinned Photodiode CMOS Image Sensor Using Reverse Substrate Bias," *Sensors* **18**, p. 118, Jan. 2018.

[6] L. Amati *et al.*, "The THESEUS space mission concept: science case, design and expected performances," *Advances in Space Research* **62**, pp. 191–244, July 2018.

[7] P. R. Jorden *et al.*, "Teledyne e2v sensors optimised for ground-based and space applications," in *High Energy, Optical, and Infrared Detectors for Astronomy VIII*, SPIE, July 2018.

[8] M. Soman *et al.*, "Design and characterisation of the new CIS115 sensor for JANUS, the high resolution camera on JUICE," in *High Energy, Optical, and Infrared Detectors for Astronomy VI*, A. D. Holland and J. Beletic, eds., SPIE, July 2014.

[9] M. R. Soman *et al.*, "Proton irradiation of the CIS115 for the JUICE mission," in *UV/Optical/IR Space Telescopes and Instruments: Innovative Technologies and Concepts VII*, H. A. MacEwen and J. B. Breckinridge, eds., SPIE, Sept. 2015.

[10] C. Crews *et al.*, "Predicting the effect of radiation damage on dark current in a space-qualified high performance CMOS image sensor," *Journal of Instrumentation* **14**, pp. C11008–C11008, Nov. 2019.

[11] I. Moody *et al.*, "CCD QE in the Soft X-ray Range," *e2v Technologies white paper* , 2017.

[12] J. Heymes *et al.*, "Comparison of back-thinned detector ultraviolet quantum efficiency for two commercially available passivation treatments," *IEEE Transactions on Nuclear Science* **67**, pp. 1962–1967, Aug. 2020.

[13] S. Sze and K. K. Ng, *Physics of Semiconductor Devices*, John Wiley & Sons, Inc., Apr. 2006.

[14] "Synopsys Sentaurus TCAD." https://www.synopsys.com/silicon/tcad.html. Accessed: 16 Aug. 2020.